Phase transitions in jalpaite, Ag_3CuS_2

2008 J. Phys.: Condens. Matter 20 455204

(http://iopscience.iop.org/0953-8984/20/45/455204)

J. Phys.: Condens. Matter **20** (2008) 455204 (10pp) doi:10.1088/0953-8984/20/45/455204

Phase transitions in jalpaite, Ag_3CuS_2

D M Trots[1,2,6], A Senyshyn[2,3], D A Mikhailova[2,4], T Vad[5] and H Fuess[2]

[1] Hamburger Synchrotronstrahlungslabor HASYLAB am Deutschen Elektronen-Synchrotron DESY, Notkestraße 85, 22607 Hamburg, Germany
[2] FB Material- und Geowissenschaften, FG Strukturforschung, Technische Universität Darmstadt, Petersenstraße 23, 64287 Darmstadt, Germany
[3] Forschungsneutronenquelle Heinz Maier-Leibnitz (FRM II), Technische Universität München, 85747 Garching, Germany
[4] Leibniz-Institut für Festkörper- und Werkstoffforschung, Helmholtzstrasse 20, 01069 Dresden, Germany
[5] Institut für Werkstoffwissenschaft, Technische Universität Dresden, Mommsenstrasse 13, 01062 Dresden, Germany

E-mail: d_trots@yahoo.com

Received 18 July 2008, in final form 15 September 2008
Published 13 October 2008
Online at stacks.iop.org/JPhysCM/20/455204

Abstract

Ag_3CuS_2 is comprehensively studied by applying synchrotron and neutron powder diffraction as well as thermal analysis in the range from 2 K up to the melting point around 960 K. The unique sequence of the reversible phase transitions P-based $\overset{110\ \mathrm{K}}{\longleftrightarrow} I4_1/a \overset{250\ \mathrm{K}}{\longleftrightarrow} I4_1/amd \overset{387\ \mathrm{K}}{\longleftrightarrow} Im\bar{3}m \overset{483\ \mathrm{K}}{\longleftrightarrow} Im\bar{3}m + Fm\bar{3}m \overset{549\ \mathrm{K}}{\longleftrightarrow} Fm\bar{3}m$ was detected prior to the sample's melting. The transitions at 110, 387 and 483–549 K are found to be of first order, whereas the transition at 250 K is a second-order one. The major change in the structure of jalpaite resulting from the $I4_1/amd \overset{250\ \mathrm{K}}{\longleftrightarrow} I4_1/a$ phase transition is a modification in the coordination geometry of the silver atoms. A large degree of structural disorder is stated for $Fm\bar{3}m$- and $Im\bar{3}m$-structured Ag_3CuS_2, which correlates with the high ionic conductivity within both cubic polymorphs. The thermal expansion of jalpaite shows some unusual features, i.e. a negative expansion along the c-direction in the $I4_1/amd$ phase, a nonlinear expansion within the $Im\bar{3}m$ polymorph and an expansion increase upon entering the mixed $Im\bar{3}m + Fm\bar{3}m$ region. Low-temperature specific heat data confirm first- and second-order anomalies at 110 and 250 K, respectively, and illustrate a pronounced non-Debye-like behaviour of jalpaite.

1. Introduction

Trisilver copper sulfide, Ag_3CuS_2 (mineral name jalpaite), is an important member of the family of silver- and copper-based chalcogenides that have attracted considerable attention due to their exceptional ion transport properties [1, 2]. Generally, these materials exhibit very high cation conductivity in high-temperature superionic phases. The ionic conductivities in the superionic face-centred cubic (fcc) phases of the $(Ag_xCu_{1-x})_2S$ system in the composition range from 20 to 80 mol% Ag_2S possess values higher than 1 Ω^{-1} cm^{-1} and demonstrate negligible dependence on temperature [3]. Furthermore, an implementation of jalpaite as an ion-selective electrode membrane for the environmental monitoring of copper ion activity in marine waters is of considerable interest [4, 5].

The earliest studies on the phase relations in the Cu–Ag–S system were performed by Djurle [6] and Skinner [7]. Ag_3CuS_2 was investigated at a limited number of temperatures in Djurle's work [6], which reports a tetragonal structure for jalpaite with a body-centred unit cell at room temperature (RT). It transforms at 385 K into a body-centred cubic (bcc) lattice and, thereafter, undergoes a transition at about 573 K into a fcc phase [6]. The fact that the a-axis of the tetragonal phase expands and the c-axis contracts upon heating was also mentioned in [6]. This indicates that the structure becomes more cubic with increasing temperature [8]. The works of Skinner [7] and Grybeck *et al* [9] were guided by mineralogical interest in jalpaite. According to [7],

[6] Author to whom any correspondence should be addressed.

jalpaite undergoes the following phase transition sequence: tetragonal $\overset{390\pm2\ \mathrm{K}}{\longleftrightarrow}$ bcc $\overset{\text{not\_defined}}{\longleftrightarrow}$ bcc + fcc $\overset{578\pm10\ \mathrm{K}}{\longleftrightarrow}$ fcc. The space group of jalpaite was determined at RT as $I4_1/amd$ [9]. This symmetry was later confirmed by electron diffraction and the structure was solved by x-ray powder diffraction [8].

To our knowledge, the structural behaviour of jalpaite has not yet been investigated at low temperatures. Besides, more accurate *in situ* powder diffraction experiments on jalpaite at non-ambient conditions are required for further theoretical and experimental studies. The present paper is therefore devoted to the investigation of Ag_3CuS_2 in a wide temperature range by thermal analysis and powder diffraction.

2. Experimental details

The Ag_3CuS_2 sample was synthesized *via* a solid-state route in evacuated sealed tubes at 1273 K from the respective chemical elements. Preliminary x-ray diffraction examinations were performed using an STOE STADI P diffractometer (Mo Kα_1 radiation, curved Ge(111) monochromator, transmission mode, step size 0.03° (2θ), curved position sensitive detector). Difference scanning calorimetry (DSC) of the sample in the temperature range of 95–298 K was performed using a DSC 204 Phoenix (Netzsch) with sealed aluminium crucibles at heating/cooling rates of 2 K min^{-1}. The high-temperature DSC measurements were performed in argon atmosphere. The sample was placed in a corundum crucible when using the Netzsch DSC 404. The temperature range of RT-1100 K was investigated using heating/cooling rates of 10 K min^{-1}. The constant pressure heat capacity was measured in the 2–300 K temperature range during the heating using a PPMS calorimeter (Quantum Design) operating via a relaxation principle.

In situ structural studies in the temperature range of 15–1025 K were performed at the synchrotron facility HASYLAB/DESY (Hamburg, Germany) with the powder diffractometer at beam-line B2 [10]. Both low- and high-temperature diffraction experiments were performed in Debye–Scherrer capillary geometry (0.3 mm quartz capillaries) using a closed-cycle cryostat [11] and a STOE furnace, respectively. All diffraction patterns were collected at fixed temperatures during the heating cycles using an image-plate detector [12] (2θ range 4°–61°). For the high-temperature measurements, a quartz capillary was filled under argon atmosphere with powdered Ag_3CuS_2 and sealed. One additional check-pattern was taken at RT after the heat treatment. For the high-temperature experiments, a wavelength of 0.640 71 Å was chosen, whereas for the low-temperature measurements, a wavelength of 0.498 99 Å was selected using a Si(111) double flat-crystal monochromator. The x-ray wavelengths were determined from eight reflection positions of LaB_6 reference material (NIST SRM 660a).

Complementary high-temperature neutron diffraction data were collected at the research neutron reactor FRM-II (Garching near Munich, Germany) at the structure powder diffractometer SPODI [13]. The powdered sample was filled into a cylindrical can of 8 mm diameter made from a thin (0.1 mm) vanadium foil. The can with the sample was mounted in a high-temperature vacuum furnace equipped with an Nb heating element. The temperature was measured simultaneously by two W/Re thermocouples and controlled with a EUROTHERM. A take-off angle of 155° was selected for the vertically focusing Ge(551) composite monochromator and the wavelength was determined to 1.548 Å by Rietveld refinement of a diffraction pattern of the silicon reference material (NIST SRM 640b). Full patterns were collected at 473 and 799 K over a 2θ range of 4°–150° with a step size of 0.05°.

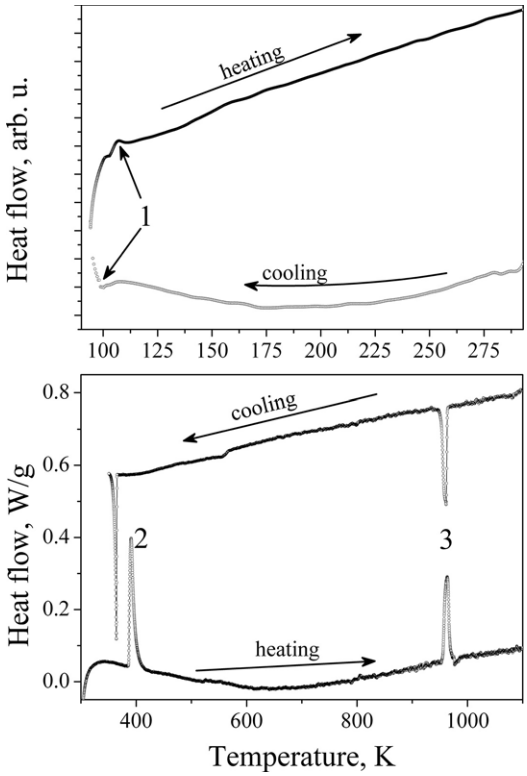

Figure 1. DSC results for Ag_3CuS_2 in the ranges of 95–298 K and 298–1100 K. 1 and 2—events which correlate with abrupt solid–solid structural transitions revealed by diffraction at 110 K and 387 K; 3—peaks which correspond to the melting point.

All diffraction patterns were analysed either by full-profile Rietveld refinements or Le Bail fits, using the software package WinPLOTR [14].

3. Results and discussion

3.1. Preliminary DSC-characterization

The low-temperature DSC measurements show endothermic and exothermic events upon heating and cooling, respectively (marked as '1' in figure 1). Some hysteresis is observed between the maxima of these signals with peak positions at 107 K on heating and 99 K on cooling. As will be described in section 3.2, these events correspond to a discontinuous structural transformation in the sample.

The high-temperature DSC heating curve of Ag_3CuS_2 in argon exhibits two pronounced endothermic peaks (marked as 2 and 3 in figure 1) with maxima at 390 and 963 K. The DSC

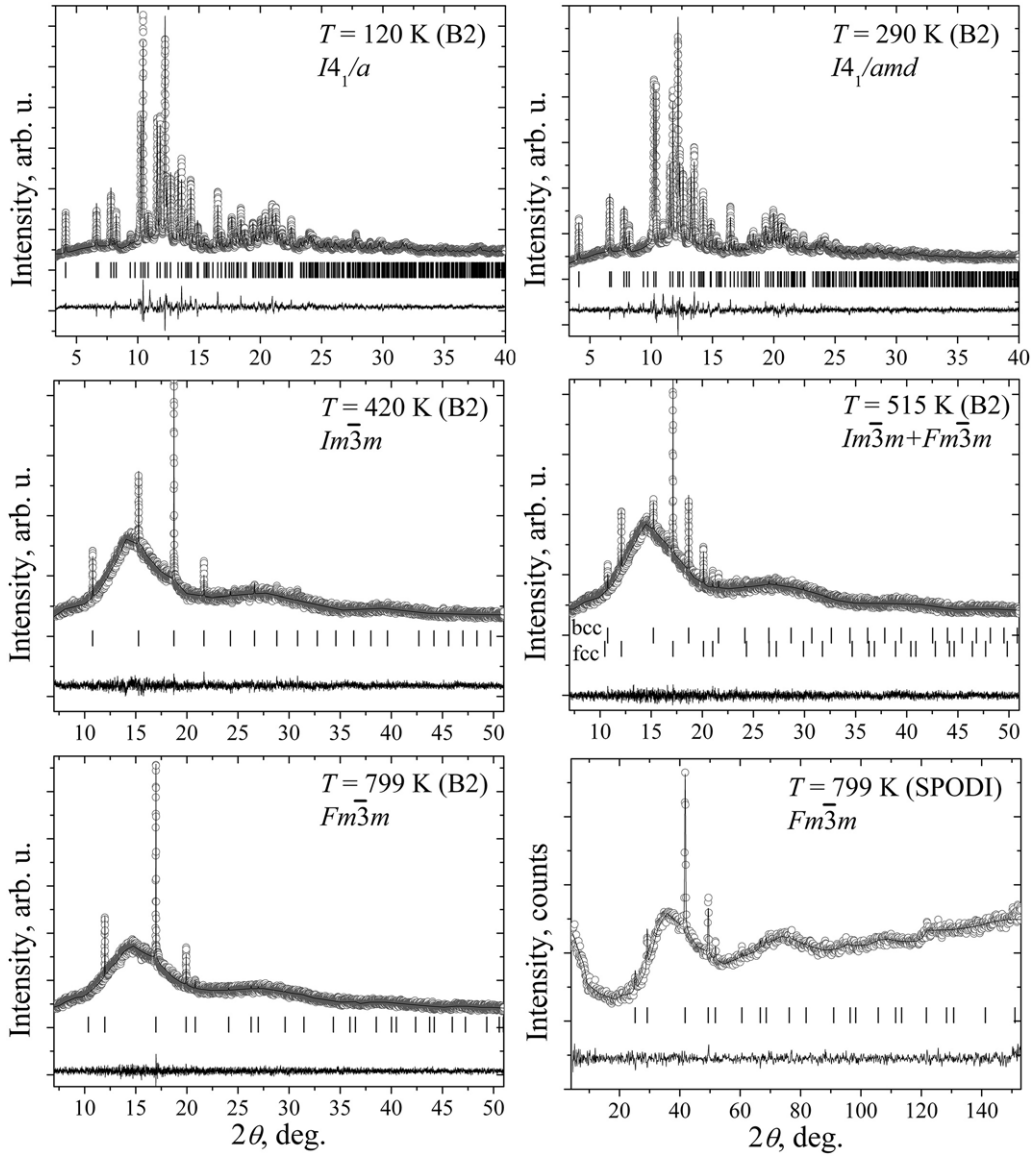

Figure 2. Results of Rietveld and Le Bail (for the bcc phase only) fits for data collected from different polymorphs of Ag_3CuS_2: circles are experimental data, the lines through the circles are the calculated profiles and the lower curves their difference. Tick marks show the calculated positions of Ag_3CuS_2 reflections. Patterns from fcc-Ag_3CuS_2 measured at B2 and SPODI were treated simultaneously.

data during successive cooling show exothermic thermal events at 364 and 960 K, i.e. some hysteresis in comparison to heating. These thermal effects correspond to abrupt structural changes in the sample and correlate with the superionic phase transition and the melting of the sample (see section 3.3).

3.2. Structural studies in the temperature range of 15–387 K

Our structural investigation of jalpaite at RT is in excellent agreement with the results of Baker *et al* [8]: the symmetry is tetragonal $I4_1/amd$ with eight formula units per cell, $Z = 8$. However, the 0.2 % difference in the unit cell volumes at RT between our (881.55(1) Å^3) and Baker's (883.88 Å^3) data can presumably be associated with a deviation from stoichiometry and an offset due to different experimental setups. As a check on the stoichiometry, occupancies of the cations were refined and, thereafter, fixed to the initial values because the deviation from the ideal compositions Ag_3CuS_2 was small. The observed, calculated and difference profiles from the final Rietveld refinement at RT are shown in figure 2. Results of refinements are summarized in tables 1 and 2. Several very weak reflections are observed in addition to those from Ag_3CuS_2. They can be assigned to a tiny amount of $(Ag, Cu)_2S$ (mineral Mckinstryite, PDF-2 card [19–406]) and are not included in the calculated diffraction pattern. Note that the structure of Mckinstryite is not yet solved.

The RT structure is based on the distorted body-centred sulfur packing and exhibits two distinct silver sites with two-fold sulfur coordination. Ag1-S and Ag2-S distances obtained from our analysis equal to 2.530(3) and 2.552(3) Å, respectively, and coincide well with the value of 2.51 Å calculated from the sum of the Shannon radii of sulfur and two-fold coordinated silver. There are also four other sulfurs

Table 1. Structure parameters of jalpaite at 290 and 120 K.

Temperature (K)	290	120
Space group	$I4_1/amd$	$I4_1/a$
a (Å)	8.6476(5)	8.6200(3)
c (Å)	11.7883(8)	11.7091(5)
V (Å^3)	881.54(9)	870.04(6)
Z	8	8
Ag1 site	8(c)	8(c)
x	0	0
y	0	0
z	0	0
u_{iso} (Å^2)	0.041(1)	0.0148(6)
Occupancy (%)	100	100
Ag2 site	16(g)	16(f)
x	−0.3127(1)	0.2826(2)
y	−0.0627(1)	0.0925(2)
z	7/8	0.8560(1)
u_{iso} (Å^2)	0.0374(7)	0.0138(4)
Occupancy (%)	100	100
Cu site	8(e)	8(e)
x	0	0
y	1/4	1/4
z	0.5319(3)	0.4688(2)
u_{iso} (Å^2)	0.028(1)	0.0019(8)
Occupancy (%)	100	100
S site	16(h)	16(f)
x	0	0.0129(6)
y	−0.0023(5)	0.0018(5)
z	0.2146(3)	0.2177(2)
u_{iso} (Å^2)	0.004(1)	0.001
Occupancy (%)	100	100
R_B (%)	7.8	6.9
R_F (%)	8.6	5.3
χ^2	11.8	16.3

Table 2. Selected bond distances and angles of the jalpaite structure at 120 and 290 K. Distances and angles are given in Å and degrees, respectively.

Ag_3CuS_2 at 120 K		Ag_3CuS_2 at 290 K	
Ag1–S × 2	2.552(2)	Ag1–S × 2	2.530(3)
Ag1–S × 2	2.983(5)	Ag1–S × 4	3.072(3)
Ag1–S × 2	3.139(5)	⟨Ag–S⟩$_6$	2.891
⟨Ag–S⟩$_6$	2.891	Ag1–Ag2 × 4	3.1271(9)
Ag1–Ag2 × 2	3.068(2)	Ag1–Cu × 2	3.359(3)
Ag1–Ag2 × 2	3.215(2)	Ag1–Ag1 × 4	4.2465(2)
Ag1–Cu × 2	3.347(2)		
Ag1–Ag1 × 4	4.2258(1)	Ag2–S × 2	2.552(3)
		Ag2–S × 2	2.957(2)
Ag2–S × 1	2.527(4)	⟨Ag–S⟩$_4$	2.755
Ag2–S × 1	2.551(3)	Ag2–Cu × 2	2.944(2)
Ag2–S × 1	2.810(5)	Ag2–Ag2 × 2	3.1404(5)
Ag2–S × 1	3.142(4)		
⟨Ag–S⟩$_4$	2.757	Cu–S × 2	2.1822(2)
Ag2–Cu × 1	2.817(2)	Cu–Cu × 1	3.699(5)
Ag2–Cu × 1	2.923(2)	S–S × 2	3.693(5)
Ag2–Cu× 1	3.093(2)		
Ag2–Ag2× 2	3.162(2)	S–Ag1–S	81.872(6)
		S-Ag1–S	98.128(6)
Cu–S × 2	2.173(5)	S-Ag1–S	88.423(6)
Cu–Cu× 1	3.659(3)	S–Ag1–S	91.577(1)
S–S × 2	3.727(6)		
		S–Ag2–S	145.936(6)
S–Ag1–S	95.7(1)	S–Ag2–S	105.89(2)
S–Ag1–S	84.3(1)	S–Ag2–S	100.59(1)
S–Ag1–S	81.1(1)	S–Ag2–S	105.89(1)
S–Ag1–S	98.9(1)	S–Ag2–S	77.281(5)
S–Ag1–S	91.2(1)	S–Ag2–S	100.591(5)
S–Ag1–S	88.8(1)		
		S–Cu–S	177.883(2)
S–Ag2–S	77.3(1)		
S–Ag2–S	110.0(1)		
S–Ag2–S	108.0(1)		
S–Ag2–S	92.4(1)		
S–Ag2–S	99.9(1)		
S–Ag2–S	141.7(1)		
S–Cu–S	179.4(2)		

at distances of 3.072(3) Å from silver in the first site. These distances are longer than the value of 2.84 Å calculated from the sum of Shannon radii of sulfur and four-fold coordinated silver. In addition to two sulfurs at 2.552(3) Å, silver in the second site is surrounded by another two sulfurs at distances of 2.957(2) Å. Thus, the silver coordination is close to either octahedral in the first site or a tetrahedral in the second. Baker *et al* [8] had therefore considered distorted octahedral and distorted tetrahedral surroundings as 'real' coordination for silver in the first and second sites, respectively. Following the notation for Ag_3CuS_2 in reference [8], we will further imply that in one site, silver has a [2 + 4] distorted octahedral sulfur environment, i.e. the distances to the two apical and to the four equatorial sulfur atoms are 2.530(3) and 3.072(3) Å, respectively. In analogy, in the second site, silver has a distorted tetrahedral [2 + 2] environment and is coordinated by two pairs of sulfur atoms at 2.552(3) and 2.957(2) Å. Copper is almost linearly coordinated by two sulfur atoms with a Cu–S distance of 2.1822(2) Å.

A simple visual analysis of the diffraction patterns collected from jalpaite reveals a continuous appearance of some additional Bragg peaks starting from 240 K down to 120 K (figure 3). The temperature of the transition was determined to 250 K. These additional reflections were successfully indexed in the same I-centred tetragonal cell containing eight formula units with the lattice parameters $a = 8.6200(3)$ and $c = 11.7091(5)$ Å at 120 K. No thermal effects were observed in the DSC curve in the vicinity of 250 K, and the temperature dependence of the cell volume indicates a linear behaviour without any abrupt changes in the range of 120–290 K. This is strong evidence for a second-order phase transition. Therefore, the possible symmetries for jalpaite in the range of 120–250 K can be described by the maximal tetragonal non-isomorphic subgroups of the space group $I4_1/amd$, i.e. $I\bar{4}2d$, $I\bar{4}m2$, $I4_1md$, $I4_122$ or $I4_1/a$. In addition, the appearance of the (114) diffraction peak indicates, that the condition $2h + l = 4n$ for the presence of a glide plane d parallel to (110) in the space group is not fulfilled; hence, the glide plane d is lost at the transition. This limits the possible symmetries to three space groups $I\bar{4}m2$, $I4_122$ and $I4_1/a$. The structural model based on the $I4_1/a$ symmetry gave the best agreement between calculated and observed profiles (figure 2). The structural parameters, bond distances and angles of jalpaite at 120 K are summarized in tables 1 and 2.

Projections of the jalpaite structure at 120 K viewed from close to the [010] direction as well as the coordination

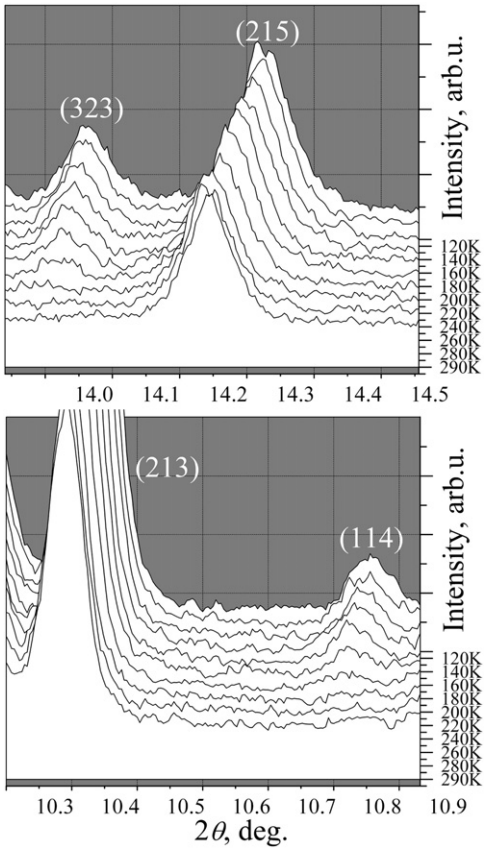

Figure 3. Temperature evolution of (114) and (323) diffraction lines in the range from RT down to 120 K.

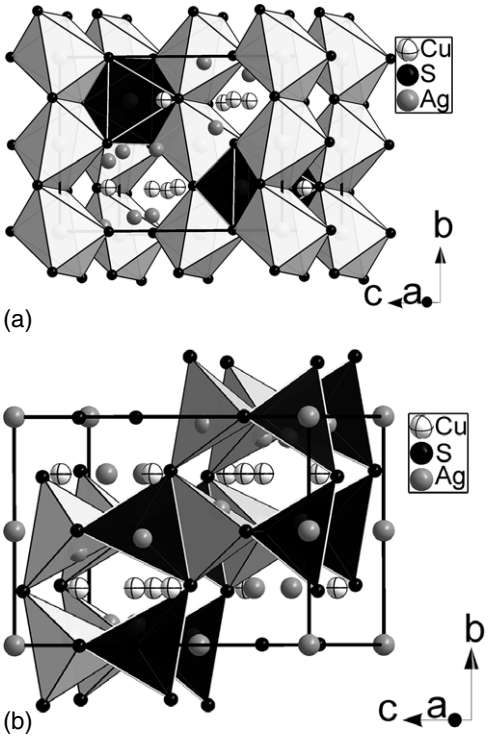

Figure 4. Structure of the $I4_1/a$-structured polymorph of jalpaite at 120 K: views in the distorted sulfur octahedra around Ag1 (a) and highly distorted tetrahedra around Ag2 (b).

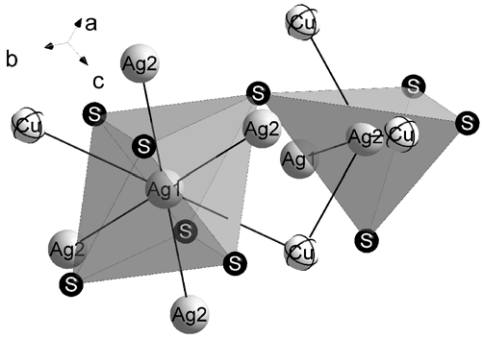

Figure 5. Distorted octahedral and tetrahedral environments of Ag1 and Ag2 in the $I4_1/a$-structured jalpaite.

environments of silver in different sites are presented in figures 4 and 5. The major change in the structure of jalpaite resulting from the $I4_1/amd \overset{250\ K}{\longleftrightarrow} I4_1/a$ phase transition is a modification in the coordination geometry of silver atoms. Similarly to the situation at RT, the structure at 120 K adopts two distinct silver sites. The four equatorial Ag1–S bond distances, which have been equal among the [2 + 4] distances of the distorted sulfur octahedron in the $I4_1/amd$ structure, split into two shorter and two longer distances in the $I4_1/a$ structure. Thus, silver in the first (Ag1) site is surrounded by a distorted [2 + 2 + 2] octahedron (figure 5), i.e. Ag1 is linearly coordinated by two pairs of equatorial sulfur atoms at 2.983(5) and 3.139(5) Å and two apical sulfur atoms at 2.552(2) Å. The Ag1 site is also linearly coordinated by two pairs of Ag2 atoms at 3.068(2) and 3.215(2) Å, respectively, and linearly surrounded by two copper atoms at 3.347(2) Å (see figure 5). Instead of the [2+2] tetrahedral environment in the $I4_1/amd$ structure, the second silver site in the $I4_1/a$ structure adopts a highly distorted coordination by four sulfur atoms at 2.527(4), 2.551(3), 2.810(5) and 3.142(4) Å. Furthermore, three different Ag2–Cu distances at 2.817(2), 2.923(2) and 3.093(2) Å as well as one Ag2–Ag1 distance at 3.068(2) Å are present in the structure (figure 5). In agreement with the $I4_1/amd$ structure, copper is almost linearly coordinated in the $I4_1/a$ structure by two sulfur atoms with a Cu–S distance of 2.173(5) Å.

The temperature dependencies of the selected interatomic distances in figure 6 reflect the structural peculiarities of two modifications of jalpaite and the changes occurring at the $I4_1/amd \overset{250\ K}{\longleftrightarrow} I4_1/a$ phase transition. Two of the equatorial Ag1–S distances within the set of [2 + 2 + 2] in the $I4_1/a$ structure clearly increase with increasing temperature, whereas the other two Ag1–S equatorial distances change only moderately (see figure 6(a)). This behaviour results in the 'convergence' of these two pairs of distances into the four equal equatorial Ag1–S distances within the [2 + 4] silver octahedron in the $I4_1/amd$ structure through the phase transition at 250 K. Figure 6(b) shows that the two apical Ag1–S distances are practically temperature independent in the $I4_1/a$ and $I4_1/amd$ structures. The two Ag2–S distances exhibit only a modest temperature dependence, as shown in figure 6(d). On the other hand, the third Ag2–S distance

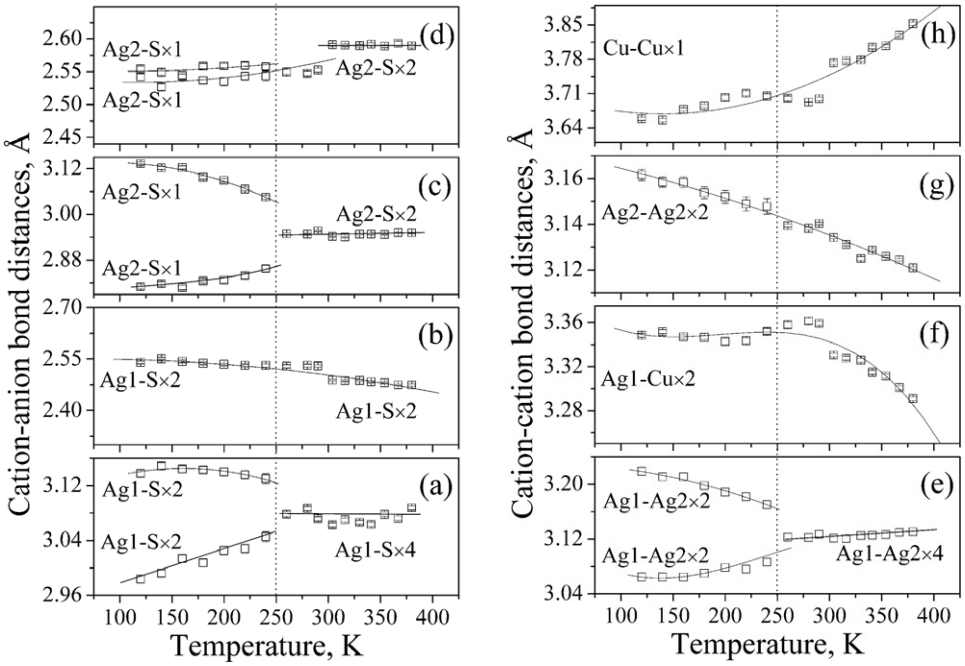

Figure 6. Temperature dependencies of selected cation–anion ((a)–(d)) and cation–cation ((e)–(h)) interatomic distances in Ag_3CuS_2 structure in the range of 120–380 K. The vertical dotted line represents the temperature of $I4_1/a \overset{250\ \mathrm{K}}{\longleftrightarrow} I4_1/amd$ phase transition. The sudden change in these dependencies at RT is the result of an offset introduced by the different sample environment used, i.e. cryostat and high-temperature furnace. Full lines are guides to the eye.

from this four-fold coordination increases with increasing temperature and, simultaneously, the fourth longer Ag2–S bond distance is reduced (see figure 6(c)). This leads to the change of the highly distorted [1 + 1 + 1 + 1] four-fold coordination of Ag2 in the $I4_1/a$ structure into the [2 + 2] tetragonal one in the $I4_1/amd$ structure through the phase transition at 250 K. Besides, the same 'convergence' behaviour is observed for the four Ag1–Ag2 distances: two of them expand as the temperature increases whereas the other two distances become smaller in the $I4_1/a$ structure, which results in the four equal Ag1–Ag2 distances in the $I4_1/amd$ structure (figure 6(e)). A decrease and increase of the Ag2–Ag2 and Cu–Cu interatomic distances with a temperature increase is observed in the whole temperature range investigated (see figures 6(g) and (h)). The two bond distances Ag1–Cu do change only slightly with increasing temperature in the range 120–290 K whereas in the successive range 290–388 K a sudden decrease is observed (see figure 6(f)).

In addition, drastic changes in the diffraction pattern, which correlate well with the DSC signal around 105 K, are observed at temperatures starting from 110 K. This is clear evidence for an abrupt transition. The diffraction patterns of this new lowest-temperature phase were indexed based on the orthorhombic primitive cell, which might be related to the I-centred tetragonal one through $b_{\mathrm{orth}} \approx a_{\mathrm{orth}} \approx 2^{0.5} \times a_{\mathrm{tetr}}$ and $c_{\mathrm{orth}} \approx c_{\mathrm{tetr}}$ with $Z = 16$ ($a_{\mathrm{orth}} = 12.1770(6)$, $b_{\mathrm{orth}} = 12.2648(6)$ and $c_{\mathrm{orth}} = 11.6409(5)$ Å at 15 K). The lattice parameters of jalpaite below 120 K were determined by a structure independent (Le Bail) full-profile decomposition. Despite powder diffraction experiments providing full-width-at-half-maxima (FWHM) of Bragg reflections ranging from 0.045 up to 0.07°, attempts of an *ab initio* determination of such a complex crystal structure were restricted by the available image-plate diffraction data. Therefore, high-resolution (FWHM ∼ 0.007–0.01°) powder diffraction experiments are required.

3.3. Structural aspects of Ag_3CuS_2 in the superionic state

The analysis of the structural behaviour of Ag_3CuS_2 shows the following phase boundaries at elevated temperatures: $I4_1/amd \overset{387\ \mathrm{K}}{\longleftrightarrow} Im\bar{3}m \overset{483\ \mathrm{K}}{\longleftrightarrow} Im\bar{3}m + Fm\bar{3}m \overset{549\ \mathrm{K}}{\longleftrightarrow} Fm\bar{3}m$. A large decrease in the peak intensities after the $I4_1/amd \overset{387\ \mathrm{K}}{\longleftrightarrow} Im\bar{3}m$ phase transformation indicates a high degree of structural disorder introduced. Furthermore, the large diffuse background in bcc- and fcc-Ag_3CuS_2 is clearly observed in both synchrotron and neutron diffraction patterns. The temperature of the tetragonal $\overset{387\ \mathrm{K}}{\longleftrightarrow}$ bcc phase boundary is in good agreement with the results presented in [6] (385 K) and [7] (390(2) K) and our DSC investigation, whereas our value for the temperature of the bcc + fcc − fcc phase boundary lies somewhat below the literature values (573 K [6] and 578(10) K [7]). This difference might be explained by some kinetic effects due to different heating rates and environmental conditions during high-temperature diffraction. No effects corresponding to the bcc + fcc − fcc phase boundary were observed in the DSC curve. Note that the temperature of the bcc − bcc + fcc boundary has not yet been mentioned in the literature. The analysis of the diffraction check-pattern from the sample after the heat treatment in argon

during the diffraction measurements shows no changes with respect to the initial state.

The systematics of the phase transitions of related copper- and silver-based superionics was considered by Hull *et al* [15], where the disordered fcc structure (or related hcp structure) was suggested to be always the lower-temperature modification, with the bcc α-AgI-like structure occurring at the highest temperature. Despite this assumption, the fcc structure was found to be the high-temperature phase for Ag_2S in a reference [15] which was stated to be anomalous. Hence, Ag_3CuS_2 is one more compound which exhibits unusual phase sequences with an fcc structure as the highest-temperature phase. The high-temperature phase sequence of jalpaite is also emphasized from an another point of view. The body-centred arrangement of sulfur in both non-superionic tetragonal ($I4_1/amd$) and superionic cubic ($Im\bar{3}m$) phases of Ag_3CuS_2 implies that the first superionic $I4_1/amd \overset{387\ \mathrm{K}}{\longleftrightarrow} Im\bar{3}m$ transformation is due to cation disorder, whereas a rearrangement of the rigid anion sublattice from body-centred to face-centred accompanies the second superionic $Im\bar{3}m \overset{483\ \mathrm{K}}{\longleftrightarrow} Im\bar{3}m + Fm\bar{3}m \overset{549\ \mathrm{K}}{\longleftrightarrow} Fm\bar{3}m$ transformation. Hence, the superionic transitions in Ag_3CuS_2 have a different origin. According to [16], there are only a few examples of structural phase transitions between two superionic phases accompanied by a rearrangement of the rigid anion sublattice. In the case of such a transition in Ag_3CuS_2 (bcc $\leftrightarrow$ fcc), investigations of the influence of different types of rigid anion sublattices on the ionic conductivity could further elucidate the relationship between superionic conductivity and underlying crystal structure.

The so-called 'split-site' analysis [2], which is a parametrization of the cation distribution using different structural models where the cations are randomly distributed over available interstitial sites within the rigid anion bcc or fcc frameworks, was used to describe the disorder in bcc- and fcc-Ag_3CuS_2. We applied simultaneous Rietveld refinements based on synchrotron and neutron diffraction data collected from the superionic phases of Ag_3CuS_2. Such refinements should give a more accurate description for the average structure due to the reduced number of refined structural parameters. During the refinements great care was taken to ensure that the data were not overinterpreted by models with an inappropriately large number of highly correlated structural parameters.

3.3.1. bcc-Ag_3CuS_2. We have attempted to model the cation distribution in bcc-Ag_3CuS_2 using different structural models with silver and copper cations randomly distributed over tetrahedral, octahedral and trigonal interstitial sites within a rigid sulfur bcc sublattice. Neutron and synchrotron diffraction data collected at 473 K were used. The refinements were based on $Im\bar{3}m$ symmetry with the S^{2-} located in the 2(a) sites at (0, 0, 0). The following models with Ag^+ and Cu^+ distributed over different cavities were tested: 12(d) tetrahedral sites at (1/4, 0, 1/2); 6(b) octahedral sites at (1/2, 1/2, 0); 24(h) trigonal sites at (x, x, 0) with $x \sim 3/8$; 6(b) octahedral sites at (1/2, 1/2, 0) and 12(d) tetrahedral sites at (1/4, 0, 1/2); 6(b) octahedral sites at (1/2, 1/2, 0) and 24(h) trigonal sites at (x, x, 0) with $x \sim 3/8$; 12(d) tetrahedral sites at (1/4, 0, 1/2) and 24(h) trigonal sites at (x, x, 0) with $x \sim 3/8$. All these models were unstable in the refinement due to high correlations between the fitted parameters and produced very poor fits to the experimental data. Thus, the results demonstrate a considerable degree of cation disorder in superionic bcc-Ag_3CuS_2, however, preferred directions of cation disorder (i.e. preferred directions for cation diffusion between available interstitial cavities in the bcc rigid cage) could not be revealed based even on neutron diffraction data.

3.3.2. fcc-Ag_3CuS_2. Table 3 shows different site models used to describe the cation disorder in fcc-Ag_3CuS_2. Simultaneous Rietveld refinements were based on a $Fm\bar{3}m$ symmetry. First of all, attempts were made to refine the data in the ideal antifluorite structure and in a 'one-site' model with cations distributed in ⟨111⟩ directions in displaced tetrahedral 32(f) sites at (x, x, x) with $1/4 < x < 1/3$ (models 1 and 2 from table 3). An improved agreement in the refinements based on models 1 and 2 from table 3 was obtained by a variation of the cation site occupancies (see models 3 and 4). A lower copper content than estimated from stoichiometry was then obtained. This is a clear indication of disorder but does not give any information about the actual cation positions. Furthermore, the following models with cations distributed between two sites were tested: between 8(c) sites at (1/4, 1/4, 1/4) and 4(b) at (1/2, 1/2, 1/2) as well as between 8(c) at (1/4, 1/4, 1/4) and 32(f) at (x, x, x) with $1/3 < x < 1/2$ (illustrating cation disorder in the ⟨111⟩ direction); between 8(c) at (1/4, 1/4, 1/4) and 48(i) at (x, x, 1/2) with $1/3 < x < 1/2$ sites (illustrating cation disorder in the ⟨110⟩ direction). Since convergence was not reached for the models with cations distributed between 8(c) in (1/4, 1/4, 1/4) and 24(d) in (0, 1/4, 1/4) positions (illustrating cation disorder in the ⟨100⟩ direction) and between 32(f) in (x, x, x) with $1/4 < x < 1/3$ and 32(f) in (x, x, x) with $1/3 < x < 1/2$ (this model implies cation distribution between displaced tetrahedral and displaced octahedral sites), the results of these refinements are not presented in table 3. Models 6 and 7 slightly improve the goodness-of-fit in comparison to model 5. However, due to the limited number of measured diffraction maxima, this improvement cannot be considered as significant. On the other hand, models 6 and 7 are just extensions of model 5. Therefore, we conclude that model 5 (cations are distributed over ideal tetrahedral 8(c) and ideal octahedral 4(b) sites) describes fcc-Ag_3CuS_2 in the optimal way (see the quality of the simultaneous fit in the figure 2). The same structural model was recently reported for superionic fcc-Ag_2S [15] and fcc-$(AgI)_x$–$(PbI_2)_{1-x}$ with $x = 4/5$ and 2/3 [17].

In order to investigate the high-temperature behaviour of superionic fcc-Ag_3CuS_2, we analysed synchrotron diffraction data in the temperature range from 543 K up to the sample's melting point on the basis of the model with random occupation of the tetrahedral 8(c) site at (1/4, 1/4, 1/4) and the octahedral 4(b) site at (1/2, 1/2, 1/2). This model yields the following temperature dependence for the parameters of the average structure of fcc-Ag_3CuS_2: the temperature factors

Table 3. A summary of the possible structural models used to interpret the diffraction data for the fcc-Ag_3CuS_2 at 799 K. Refinements were based on the $Fm\bar{3}m$ symmetry ($Z = 2$, $a = 6.1403(4)$ Å). Neutron and synchrotron diffraction data were treated simultaneously. χ^2 is the goodness-of-fit. The isotropic thermal parameters u_{iso} and positional parameters of the cations as well as the cation site occupancies in 'split' positions were constrained during the refinements.

Model	1 Tetrahedral sites	2 Displaced tetrahedral sites	3 Partial occupation of tetrahedral sites	4 Partial occupation of displaced tetrahedral sites	5 Tetrahedral and octahedral sites	6 Tetrahedral and ⟨111⟩ displaced octahedral sites	7 Tetrahedral and ⟨110⟩ displaced octahedral sites
S, site				4(a) at (0, 0, 0)			
u_{iso} (Å^2)	0.014(5)	0.006(2)	0.013(7)	0.014(2)	0.19(1)	0.22(2)	0.22(2)
Occupancy (%)	100	100	100	100	100	100	100
Ag/Cu, site	8(c)	32(f)	8(c)	32(f)	8(c)	8(c)	8(c)
x	1/4	0.2962(9)	1/4	0.2984(9)	1/4	1/4	1/4
y	1/4	0.2962(9)	1/4	0.2984(9)	1/4	1/4	1/4
z	1/4	0.2962(9)	1/4	0.2984(9)	1/4	1/4	1/4
u_{iso} (Å^2)	0.089(5)	0.006(2)	0.085(5)	0.014(2)	0.70(1)	0.64(2)	0.63(2)
Occupancy (%)	100	25	74(1)	22(3)	63(2)	52(2)	52(2)
Ag/Cu, site	—	—	—	—	4(b)	32(f)	48(i)
x	—	—	—	—	1/2	0.425(7)	0.407(9)
y	—	—	—	—	1/2	0.425(7)	0.407(9)
z	—	—	—	—	1/2	0.425(7)	1/2
u_{iso} (Å^2)	—	—	—	—	0.70(1)	0.64(2)	0.63(2)
Occupancy (%)	—	—	—	—	73(3)	11.9(5)	7.9(4)
χ^2	13.1	12.6	12.5	11.7	8.52	8.46	8.46

for the cations and anions practically do not change with temperature and there are no pronounced changes in the temperature dependence of the cation occupancies. Note that diffraction results on a number of copper and silver-based chalcogenides and halides (for instance, results of [17–21]) imply that the ionic conductivity can be sensitive to details of the cation redistribution between available interstitial sites versus temperature as well as to the stoichiometry of the material. Taking this into account, we suggest a correlation between the results of the electrochemical measurements from Kadrgulov *et al* [3], which revealed only a relatively modest increase in the ionic conductivity with temperature within fcc-$(Ag_xCu_{1-x})_2S$ and our diffraction results, which show no pronounced cation redistribution. The same correlation was supposed for related superionic fcc-AgCuSe [19], fcc-AgCuS [21] and fcc-$(AgI)_x$–$(PbI_2)_{1-x}$ with $x = 4/5$ and 2/3 [17].

Doubtless, single crystal measurements of superionic bcc- and fcc-Ag_3CuS_2 would provide more information about the underlying structure. Any single crystal studies are, however, practically impossible (or at least extremely difficult) even if single crystals were available, since the first-order superionic phase transition will lead to fracture. Nevertheless, the temperature dependence of the cation redistribution in fcc-Ag_3CuS_2 as described by our structural model correlates well with the temperature behaviour of the ionic conductivity and gives strong support to the validity of the model.

3.4. Thermal expansion of jalpaite

The unit cell dimensions and unit cell volume per formula unit of jalpaite as a function of temperature are illustrated in

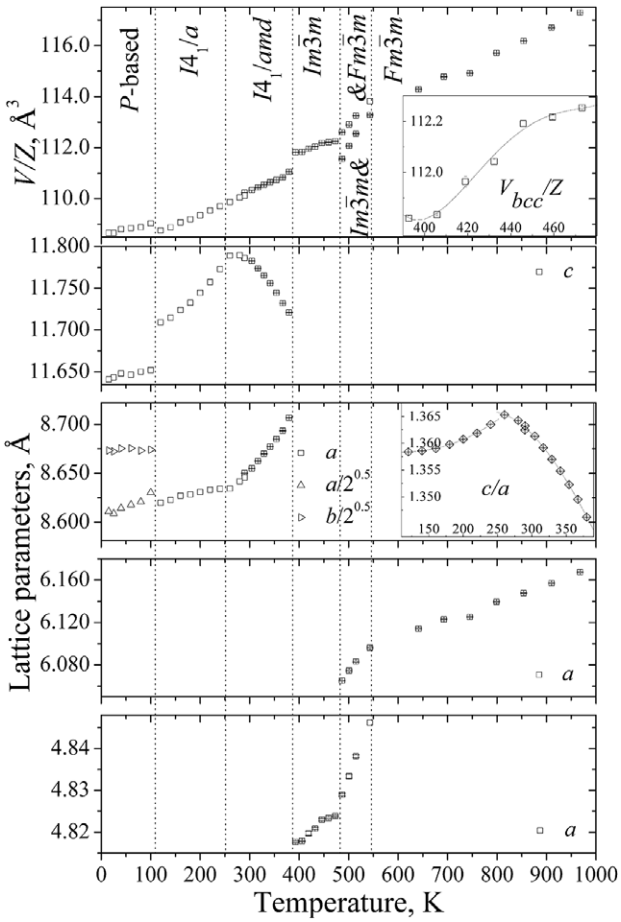

Figure 7. Behaviour of cell dimensions of jalpaite in the range from 15 K up to the melting point. Insets illustrate nonlinear thermal expansion of bcc-Ag_3CuS_2 and temperature behaviour of the c/a axial ratio within tetragonal polymorphs of Ag_3CuS_2.

figure 7. A nonlinear expansion was revealed within bcc-Ag_3CuS_2 (see inset in figure 7), whereas other polymorphic modifications of jalpaite expand linearly with increasing temperature. The volume thermal expansion coefficients for all polymorphs with the exception of the bcc-polymorph were therefore calculated from the temperature dependencies of the unit cell volume in the linear approximation and are equal to 3.89×10^{-5}, 7.33×10^{-5}, 8.57×10^{-5} and 8.22×10^{-5} K^{-1} for the lowest-temperature P-based, $I4_1/a$-structured, $I4_1/amd$-structured and fcc phases, respectively. On entering the mixed bcc + fcc region between 483 and 549 K, the thermal expansion of both phases suddenly increases. The discontinuous volume changes around 0.38% at the transition from the lowest-temperature P-based phase into the $I4_1/a$-structured jalpaite; the changes of 0.77% at the $I4_1/amd \overset{387\ K}{\longleftrightarrow}$ bcc and 0.58% at the bcc $\overset{483\ K}{\longleftrightarrow}$ bcc + fcc $\overset{549\ K}{\longleftrightarrow}$ fcc transformations are very strong indications for a first-order phase transition.

A negative thermal expansion along the c-direction is observed in $I4_1/amd$-structured jalpaite, whereas Ag_3CuS_2 expands along the c-direction within the $I4_1/a$ phase. Accordingly, an increase and decrease of the c/a axial ratio is revealed within the $I4_1/a$ and $I4_1/amd$ tetragonal polymorphs of jalpaite (see inset in figure 7), indicating anisotropic expansion. It should be noted that an anomalous thermal expansion in the non-superionic phases, which precede the superionic ones, seems to be characteristic for other superionic compounds. The negative thermal expansion in the c-direction was detected in some other superionic conductors by powder diffraction, for instance, in hexagonal β-AgI [22], β-CuI [23], α-AgCuS [21], and orthorhombic β-AgCuS [21]. The decrease in the c/a axial ratio was also reported for superionic compounds such as hexagonal β-CuI [23, 24] and α-AgCuS [21], pseudo-hexagonal orthorhombic β-Ag_2ZnI_4 [25] and β-AgCuS [21], tetragonal β-Cu_2HgI_4 [26] and is also indicated by the results in [22] for hexagonal β-AgI. An explanation of the negative thermal expansion along the c-axis of β-AgI was successfully given in terms of a coupling between a cluster pair of mobile ions and local static distortions [27, 28]. The negative thermal expansion along the c-direction in tetragonal Ag_3CuS_2 can be explained in terms of cluster-induced local distortions as well.

3.5. Specific heat capacity

In addition to the synchrotron and neutron diffraction experiments, the molar heat capacity of jalpaite was measured (see figure 8). The data display two remarkable features. The first one is a second-order anomaly at 250 K, which is in excellent agreement with the temperature of the $I4_1/a \overset{250\ K}{\longleftrightarrow} I4_1/amd$ transition determined from our diffraction results. The second one is a λ-peak with its maximum at 110 K, which correlates with thermal events observed at 107 K on heating and 99 K on cooling in the DSC curve. The λ-peak corresponds to the first-order P-based $\overset{110\ K}{\longleftrightarrow} I4_1/a$ transition revealed by the diffraction studies. Moreover, the heat capacity curve shows the absence of further

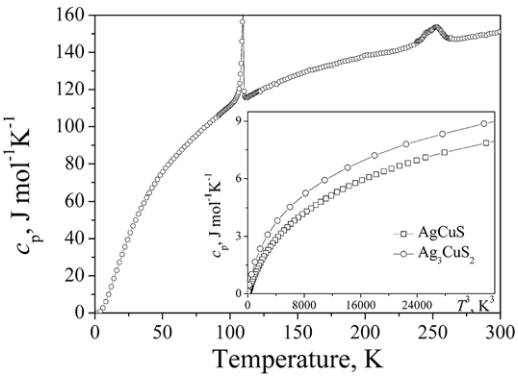

Figure 8. Low-temperature heat capacity of jalpaite. The λ-peak at 110 K corresponds to the abrupt P-based $\overset{110\ K}{\longleftrightarrow} I4_1/a$ transition, while the anomaly with its maximum at 250 K correlates with the second-order $I4_1/a \overset{250\ K}{\longleftrightarrow} I4_1/amd$ transition. Inset: $c_p(T)$ versus T^3 representation.

transitions in the range of 2–15 K, which was not covered during diffraction experiments. The inset of figure 8 displays the specific heat of Ag_3CuS_2 and the related AgCuS (data for AgCuS are taken from [29]) below 33 K in the $c_p(T)$ versus T^3 representation. The nonlinear behaviour of these plots is particularly noteworthy. Such a nonlinearity implies that the Debye phonon model with its cubic dependence on temperature does not match the data for both compounds even at low temperatures. The non-Debye-like behaviour, which is evidence of a high level of anharmonicity in the system, was also revealed for related eucairite (AgCuSe) [19].

An interpolation of the experimental heat capacity data yields the thermodynamic standard value $c_p(298.15\ K) = 150.8\ J\ mol^{-1}\ K^{-1}$, whereas the standard values $S(298.15\ K) = 275.4\ J\ mol^{-1}\ K^{-1}$ and $\Delta H(298.15\ K) = 33.7\ kJ\ mol^{-1}$ were calculated by numerical integration of the experimental data. The enthalpy change at the P-based $\overset{110\ K}{\longleftrightarrow} I4_1/a$ transition determined from the area of the λ-peak equals 0.44 kJ mol^{-1} which is about 15 times smaller than the changes of enthalpies at the superionic $I4_1/amd \overset{387\ K}{\longleftrightarrow} Im\bar{3}m$ transition (7.0 kJ mol^{-1}) and the sample's melting (6.5 kJ mol^{-1}). Obviously the enthalpy change at the solid-state superionic transition in Ag_3CuS_2 is of the same order of magnitude as the enthalpy change at fusion. This fact agrees well with previous results for related superionic compounds such as AgI, Ag_2S, CuBr, LuF_3, YF_3 etc [30] and, in addition to the diffraction studies, illustrates that the cation sublattice melting coincides with the transition.

4. Conclusions

The unique sequence of reversible phase transitions P-based $\overset{110\ K}{\longleftrightarrow} I4_1/a \overset{250\ K}{\longleftrightarrow} I4_1/amd \overset{387\ K}{\longleftrightarrow} Im\bar{3}m \overset{483\ K}{\longleftrightarrow} Im\bar{3}m + Fm\bar{3}m \overset{549\ K}{\longleftrightarrow} Fm\bar{3}m$ was revealed in non-Debye-like jalpaite, Ag_3CuS_2. The large volume change of 0.77% at the first-order $I4_1/amd \overset{387\ K}{\longleftrightarrow} Im\bar{3}m$ transformation accompanied with a conductivity increase by two orders of magnitude at this

transition [31] shows that jalpaite undergoes a type-I superionic phase transition according to the classification of Boyce and Huberman [30], i.e. Ag_3CuS_2 transforms abruptly into the highly conducting state.

Indeed, the analysis of the average structure without considering the significant diffuse scattering did not reveal all structural details which might be of great importance for understanding the underlying conduction mechanism in superionic Ag_3CuS_2. Total scattering measurements, which include both Bragg and diffuse intensities, are therefore envisaged in the near future.

Acknowledgments

Susann Müller from the Max-Planck-Institut für Chemische Physik fester Stoffe in Dresden, M Sc Florian Schrettle from Universitaet Augsburg (Lehrstuhl für Experimentalphysik V) and B Bartusch from Leibniz Institute for Solid State and Materials Research in Dresden are gratefully acknowledged for performing the DSC measurements. We are indebted to Andreas Berghaeuser from HASYLAB/UNI Hamburg for his help in maintaining the closed-cycle cryostat. We are also grateful to Dr A N Skomorokhov from the Institute for Physics and Power Engineering, Obninsk, Russia (now at The International Foundation of Technology and Investment, Moscow, Russia), for his continuous interest throughout the last four years. Financial support from the Bundesministerium für Bildung und Forschung (grant 03DU03D1) and from the Helmholtz Association of National Research Centres (grant VH-VI 102) is gratefully acknowledged.

References

[1] Hull S 2004 *Rep. Prog. Phys.* **67** 1233–314
[2] Keen D A 2002 *J. Phys.: Condens. Matter* **14** R819–57
[3] Kadrgulov R F, Yakshibaev R A and Khasanov M A 2001 *Ionics* **7** 156–60
[4] De Marco R 1996 *Mar. Chem.* **55** 389–98
[5] Zirino A, VanderWeele D A, Belli S L, DeMarco R and Mackey D J 1998 *Mar. Chem.* **61** 173–84
[6] Djurle S 1958 *Acta Chem. Scand.* **12** 1427–36
[7] Skinner B J 1966 *Econ. Geol.* **61** 1–26
[8] Baker C L, Lincoln F J and Johnson A W S 1992 *Aust. J. Chem.* **45** 1441–9
[9] Grybeck D and Finney J J 1968 *Am. Mineral.* **53** 1530–42
[10] Knapp M, Baehtz C, Ehrenberg H and Fuess H 2004 *J. Synchrotron Radiat.* **11** 328–34
[11] Ihringer J and Küster A 1993 *J. Appl. Crystallogr.* **26** 135–7
[12] Knapp M, Joco V, Baehtz C, Brecht H H, Berghaeuser A, Ehrenberg H, von Seggern H and Fuess H 2004 *Nucl. Instrum. Methods* A **521** 565–70
[13] Hoelzel M, Senyshyn A, Gilles R, Boysen H and Fuess H 2007 *Neutron News* **18** 23–6
[14] Roisnel T and Rodriguez-Carvajal J 2001 *Mater. Sci. Forum* **378–381** 118–23
[15] Hull S, Keen D A, Sivia D S, Madden P A and Wilson M 2002 *J. Phys.: Condens. Matter* **14** L9
[16] Hull S and Keen D A 2001 *J. Phys.: Condens. Matter* **13** 5597–610
[17] Hull S, Keen D A and Berastegui P 2002 *Solid State Ion.* **147** 97–106
[18] Skomorokhov A N, Trots D M, Knapp M, Bickulova N N and Fuess H 2006 *J. Alloys Compounds* **421** 64–71
[19] Trots D M, Skomorokhov A N, Knapp M and Fuess H 2006 *Eur. Phys. J.* B **51** 507–12
[20] Keen D A, Hull S, Barnes A C, Berastegui P, Crichton W A, Madden P A, Tucker M G and Wilson M 2003 *Phys. Rev.* B **68** 014117
[21] Trots D M, Senyshyn A, Mikhailova D A, Knapp M, Baehtz C, Hoelzel M and Fuess H 2007 *J. Phys.: Condens. Matter* **19** 136204
[22] Yoshiasa A, Inaba A, Ishii T and Koto K 1995 *Solid State Ion.* **79** 67–70
[23] Keen D A and Hull S 1994 *J. Phys.: Condens. Matter* **6** 1637–44
[24] Keen D A and Hull S 1995 *J. Phys.: Condens. Matter* **7** 5793–804
[25] Hull S, Keen D A and Berastegui P 2002 *J. Phys.: Condens. Matter* **14** 13579–96
[26] Hull S and Keen D A 2000 *J. Phys.: Condens. Matter* **12** 3751–65
[27] Ishii T 1998 *Solid State Commun.* **108** 513–7
[28] Ishii T and Kamishima O 2001 *J. Phys. Soc. Japan* **70** 159–66
[29] Skomorokhov A N, Trots D M, Ovchinnikov S G and Fuess H 2007 *J. Phys.: Condens. Matter* **19** 186228
[30] Boyce J B and Huberman B A 1979 *Phys. Rep.* **51** 189–265
[31] Graf R B 1968 *J. Electrochem. Soc.* **115** 433–4